Comprehensive in vivo micro-vascular imaging of the human eye by dual-beam-scan Doppler optical coherence angiography

著者	Makita Shuichi, Jaillon Franck, Yamanari Masahiro, Miura Masahiro, Yasuno Yoshiaki
journal or publication title	Optics Express
volume	19
number	2
page range	1271-1283
year	2011-01
権利	(C)2011 Optical Society of America
URL	http://hdl.handle.net/2241/108107

doi: 10.1364/OE.19.001271

Comprehensive *in vivo* micro-vascular imaging of the human eye by dual-beam-scan Doppler optical coherence angiography

Shuichi Makita,[1,3] Franck Jaillon,[1,3] Masahiro Yamanari[1,3] Masahiro Miura,[2,3] and Yoshiaki Yasuno[1,3,*]

[1]*Computational Optics Group in University of Tsukuba, 1-1-1 Tennodai, Tsukuba, Ibaraki 3050001, Japan*
[2]*Department of Ophthalmology, Tokyo Medical University Ibaraki Medical Center, 3-20-1 Chuo, Ami, Inashiki, Ibaraki 3000395, Japan*
[3]*Computational of Optics and Ophthalmology Group, University of Tsukuba, Tsukuba, Ibaraki 3050001, Japan*
**yasuno@optlab2.bk.tsukuba.ac.jp*

Abstract: Comprehensive angiography provides insight into the diagnosis of vascular-related diseases. However, complex microvascular networks of unstable *in vivo* organs such as the eye require micron-scale resolution in three dimensions and a high sampling rate to access a wide area as maintaining the high resolution. Here, we introduce dual-beam-scan Doppler optical coherence angiography (OCA) as a label-free comprehensive ophthalmic angiography that satisfies theses requirements. In addition to high resolution and high imaging speed, high sensitivity to motion for detecting tiny blood flow of microvessels is achieved by detecting two time-delayed signals with scanning of two probing beams separated on a sample. We present *in vivo* three-dimensional imaging of the microvasculature of the posterior part of the human eye. The demonstrated results show that this technique may be used for comprehensive ophthalmic angiography to evaluate the vasculature of the posterior human eye and to diagnose variety of vascular diseases.

OCIS codes: (170.3890) Medical optics instrumentation; (170.4460) Ophthalmic optics and devices; (170.4500) Optical coherence tomography; (170.4470) Ophthalmology; (120.3340) Laser Doppler velocimetry.

References and links

1. S. Dithmar, and F. G. Holz, *Fluorescence Angiography in Ophthalmology* (Springer, 2008).
2. A. Fercher, and J. Briers, "Flow visualization by means of single-exposure speckle photography," Opt. Commun. **37**(5), 326–330 (1981).
3. G. Michelson, and B. Schmauss, "Two dimensional mapping of the perfusion of the retina and optic nerve head," Br. J. Ophthalmol. **79**(12), 1126–1132 (1995).
4. D. A. Nelson, S. Krupsky, A. Pollack, E. Aloni, M. Belkin, I. Vanzetta, M. Rosner, and A. Grinvald, "Special report: Noninvasive multi-parameter functional optical imaging of the eye," Ophthalmic Surg. Lasers Imaging **36**(1), 57–66 (2005).
5. G. D. Rubin, and N. M. Rofsky, eds., *CT and MR Angiography: Comprehensive Vascular Assessment* (Lippincott Williams & Wilkins Publishers, Philadelphia, 2008).
6. W. Drexler, and J. G. Fujimoto, eds., *Optical Coherence Tomography: Technology and Applications, Biological and Medical Physics, Biomedical Engineering* (Springer, 2008).
7. A. Fercher, C. Hitzenberger, G. Kamp, and S. El-Zaiat, "Measurement of intraocular distances by backscattering spectral interferometry," Opt. Commun. **117**(1-2), 43–48 (1995).
8. M. Wojtkowski, R. Leitgeb, A. Kowalczyk, T. Bajraszewski, and A. F. Fercher, "*In vivo* human retinal imaging by Fourier domain optical coherence tomography," J. Biomed. Opt. **7**(3), 457–463 (2002).
9. S. Yun, G. Tearney, J. de Boer, N. Iftimia, and B. Bouma, "High-speed optical frequency-domain imaging," Opt. Express **11**(22), 2953–2963 (2003).
10. N. A. Nassif, B. Cense, B. H. Park, M. C. Pierce, S. H. Yun, B. E. Bouma, G. J. Tearney, T. C. Chen, and J. F. de Boer, "*In vivo* high-resolution video-rate spectral-domain optical coherence tomography of the human retina and optic nerve," Opt. Express **12**(3), 367–376 (2004).
11. U. Schmidt-Erfurth, R. A. Leitgeb, S. Michels, B. Povazay, S. Sacu, B. Hermann, C. Ahlers, H. Sattmann, C. Scholda, A. F. Fercher, and W. Drexler, "Three-dimensional ultrahigh-resolution optical coherence tomography of macular diseases," Invest. Ophthalmol. Vis. Sci. **46**(9), 3393–3402 (2005).

#138562 - $15.00 USD Received 24 Nov 2010; revised 7 Jan 2011; accepted 9 Jan 2011; published 14 Jan 2011

12. M. Wojtkowski, V. Srinivasan, J. G. Fujimoto, T. Ko, J. S. Schuman, A. Kowalczyk, and J. S. Duker, "Three-dimensional retinal imaging with high-speed ultrahigh-resolution optical coherence tomography," Ophthalmology **112**(10), 1734–1746 (2005).
13. R. Huber, M. Wojtkowski, J. G. Fujimoto, J. Y. Jiang, and A. E. Cable, "Three-dimensional and C-mode OCT imaging with a compact, frequency swept laser source at 1300 nm," Opt. Express **13**(26), 10523–10538 (2005).
14. Y. Yasuno, V. D. Madjarova, S. Makita, M. Akiba, A. Morosawa, C. Chong, T. Sakai, K.-P. Chan, M. Itoh, and T. Yatagai, "Three-dimensional and high-speed swept-source optical coherence tomography for *in vivo* investigation of human anterior eye segments," Opt. Express **13**(26), 10652–10664 (2005).
15. S. H. Yun, G. J. Tearney, B. J. Vakoc, M. Shishkov, W. Y. Oh, A. E. Desjardins, M. J. Suter, R. C. Chan, J. A. Evans, I.-K. Jang, N. S. Nishioka, J. F. de Boer, and B. E. Bouma, "Comprehensive volumetric optical microscopy *in vivo*," Nat. Med. **12**(12), 1429–1433 (2007).
16. S. Makita, Y. Hong, M. Yamanari, T. Yatagai, and Y. Yasuno, "Optical coherence angiography," Opt. Express **14**(17), 7821–7840 (2006).
17. A. H. Bachmann, M. L. Villiger, C. Blatter, T. Lasser, and R. A. Leitgeb, "Resonant Doppler flow imaging and optical vivisection of retinal blood vessels," Opt. Express **15**(2), 408–422 (2007).
18. L. An, and R. K. Wang, "*In vivo* volumetric imaging of vascular perfusion within human retina and choroids with optical micro-angiography," Opt. Express **16**(15), 11438–11452 (2008).
19. Y. K. Tao, A. M. Davis, and J. A. Izatt, "Single-pass volumetric bidirectional blood flow imaging spectral domain optical coherence tomography using a modified Hilbert transform," Opt. Express **16**(16), 12350–12361 (2008).
20. A. Szkulmowska, M. Szkulmowski, D. Szlag, A. Kowalczyk, and M. Wojtkowski, "Three-dimensional quantitative imaging of retinal and choroidal blood flow velocity using joint Spectral and Time domain Optical Coherence Tomography," Opt. Express **17**(13), 10584–10598 (2009).
21. V. J. Srinivasan, S. Sakadzić, I. Gorczynska, S. Ruvinskaya, W. Wu, J. G. Fujimoto, and D. A. Boas, "Quantitative cerebral blood flow with optical coherence tomography," Opt. Express **18**(3), 2477–2494 (2010).
22. R. Leitgeb, L. Schmetterer, W. Drexler, A. Fercher, R. Zawadzki, and T. Bajraszewski, "Real-time assessment of retinal blood flow with ultrafast acquisition by color Doppler Fourier domain optical coherence tomography," Opt. Express **11**(23), 3116–3121 (2003).
23. B. R. White, M. C. Pierce, N. Nassif, B. Cense, B. H. Park, G. J. Tearney, B. E. Bouma, T. C. Chen, and J. F. de Boer, "In vivo dynamic human retinal blood flow imaging using ultra-high-speed spectral domain optical coherence tomography," Opt. Express **11**(25), 3490–3497 (2003).
24. B. J. Vakoc, R. M. Lanning, J. A. Tyrrell, T. P. Padera, L. A. Bartlett, T. Stylianopoulos, L. L. Munn, G. J. Tearney, D. Fukumura, R. K. Jain, and B. E. Bouma, "Three-dimensional microscopy of the tumor microenvironment *in vivo* using optical frequency domain imaging," Nat. Med. **15**(10), 1219–1223 (2009).
25. J. Fingler, R. J. Zawadzki, J. S. Werner, D. Schwartz, and S. E. Fraser, "Volumetric microvascular imaging of human retina using optical coherence tomography with a novel motion contrast technique," Opt. Express **17**(24), 22190–22200 (2009).
26. I. Grulkowski, I. Gorczynska, M. Szkulmowski, D. Szlag, A. Szkulmowska, R. A. Leitgeb, A. Kowalczyk, and M. Wojtkowski, "Scanning protocols dedicated to smart velocity ranging in spectral OCT," Opt. Express **17**(26), 23736–23754 (2009).
27. R. K. Wang, L. An, P. Francis, and D. J. Wilson, "Depth-resolved imaging of capillary networks in retina and choroid using ultrahigh sensitive optical microangiography," Opt. Lett. **35**(9), 1467–1469 (2010).
28. C. K. Hitzenberger, and A. F. Fercher, "Differential phase contrast in optical coherence tomography," Opt. Lett. **24**(9), 622–624 (1999).
29. D. P. Davé, and T. E. Milner, "Optical low-coherence reflectometer for differential phase measurement," Opt. Lett. **25**(4), 227–229 (2000).
30. M. Yamanari, S. Makita, V. D. Madjarova, T. Yatagai, and Y. Yasuno, "Fiber-based polarization-sensitive Fourier domain optical coherence tomography using B-scan-oriented polarization modulation method," Opt. Express **14**(14), 6502–6515 (2006).
31. M. K. Al-Qaisi, and T. Akkin, "Polarization-sensitive optical coherence tomography based on polarization-maintaining fibers and frequency multiplexing," Opt. Express **16**(17), 13032–13041 (2008).
32. E. Götzinger, B. Baumann, M. Pircher, and C. K. Hitzenberger, "Polarization maintaining fiber based ultra-high resolution spectral domain polarization sensitive optical coherence tomography," Opt. Express **17**(25), 22704–22717 (2009).
33. J. Salo, H. El-Sallabi, and P. Vainikainen, "The Distribution of the Product of Independent Rayleigh Random Variables," IEEE Trans. Antenn. Propag. **54**(2), 639–643 (2006).
34. M. Miura, S. Makita, T. Iwasaki, and Y. Yasuno, "Three-dimensional visualization of ocular vascular pathology by optical coherence angiography *in vivo*," Invest. Ophthalmol. Vis. Sci. (to be published).
35. A. P. Ciardella, I. M. Donsoff, S. J. Huang, D. L. Costa, and L. A. Yannuzzi, "Polypoidal choroidal vasculopathy," Surv. Ophthalmol. **49**(1), 25–37 (2004).
36. R. A. Costa, E. V. Navajas, M. E. Farah, D. Calucci, J. A. Cardillo, and I. U. Scott, "Polypoidal choroidal vasculopathy: angiographic characterization of the network vascular elements and a new treatment paradigm," Prog. Retin. Eye Res. **24**(5), 560–586 (2005).
37. M. Levoy, "Display of surfaces from volume data," IEEE Comput. Graph. Appl. **8**(3), 29–37 (1988).
38. G. A. Cioffi, E. Granstam, and A. Alm, *Adler's Physiology of the Eye: Clinical Application* (Mosby, Inc., 2003), chap. 33, p. 747, 10th ed.
39. D. Toussaint, T. Kuwabara, and D. G. Cogan, "Retinal vascular patterns. II. Human retinal vessels studied in three dimensions," Arch. Ophthalmol. **65**, 575–581 (1961).

#138562 - $15.00 USD Received 24 Nov 2010; revised 7 Jan 2011; accepted 9 Jan 2011; published 14 Jan 2011

40. Y. Zhao, Z. Chen, C. Saxer, S. Xiang, J. F. de Boer, and J. S. Nelson, "Phase-resolved optical coherence tomography and optical Doppler tomography for imaging blood flow in human skin with fast scanning speed and high velocity sensitivity," Opt. Lett. **25**(2), 114–116 (2000).
41. G. H. Bresnick, R. Condit, S. Syrjala, M. Palta, A. Groo, and K. Korth, "Abnormalities of the foveal avascular zone in diabetic retinopathy," Arch. Ophthalmol. **102**(9), 1286–1293 (1984).
42. O. Arend, S. Wolf, F. Jung, B. Bertram, H. Pöstgens, H. Toonen, and M. Reim, "Retinal microcirculation in patients with diabetes mellitus: dynamic and morphological analysis of perifoveal capillary network," Br. J. Ophthalmol. **75**(9), 514–518 (1991).
43. J. Conrath, R. Giorgi, D. Raccah, and B. Ridings, "Foveal avascular zone in diabetic retinopathy: quantitative vs qualitative assessment," Eye (Lond.) **19**(3), 322–326 (2005).
44. H. F. Zhang, K. Maslov, G. Stoica, and L. V. Wang, "Functional photoacoustic microscopy for high-resolution and noninvasive *in vivo* imaging," Nat. Biotechnol. **24**(7), 848–851 (2006).
45. J. B. Pawley, ed., *Handbook of biological confocal microscopy* (Plenum Press, New York, 1995), 2nd ed.
46. B. J. Vakoc, G. J. Tearney, and B. E. Bouma, "Statistical properties of phase-decorrelation in phase-resolved Doppler optical coherence tomography," IEEE Trans. Med. Imaging **28**(6), 814–821 (2009).
47. S. Wolf, O. Arend, K. Schulte, T. H. Ittel, and M. Reim, "Quantification of retinal capillary density and flow velocity in patients with essential hypertension," Hypertension **23**(4), 464–467 (1994).
48. M. Pircher, E. Götzinger, O. Findl, S. Michels, W. Geitzenauer, C. Leydolt, U. Schmidt-Erfurth, and C. K. Hitzenberger, "Human macula investigated *in vivo* with polarization-sensitive optical coherence tomography," Invest. Ophthalmol. Vis. Sci. **47**(12), 5487–5494 (2006).
49. B. Baumann, S. O. Baumann, T. Konegger, M. Pircher, E. Gotzinger, H. Sattmann, M. Litschauer, and C. K. Hitzenberger, "Polarization sensitive optical coherence tomography of melanin provides tissue inherent contrast based on depolarization," Proc. SPIE **7554**, 75541M, 75541M-6 (2010), https://cogrt.bk.tsukuba.ac.jp/COG/locked/yasuno/papers/BiOS2010Proceedings/DATA/7554_57.PDF.
50. B. Povazay, B. Hermann, B. Hofer, V. Kajić, E. Simpson, T. Bridgford, and W. Drexler, "Wide-field optical coherence tomography of the choroid *in vivo*," Invest. Ophthalmol. Vis. Sci. **50**(4), 1856–1863 (2008).
51. Y. Yasuno, M. Miura, K. Kawana, S. Makita, M. Sato, F. Okamoto, M. Yamanari, T. Iwasaki, T. Yatagai, and T. Oshika, "Visualization of sub-retinal pigment epithelium morphologies of exudative macular diseases by high-penetration optical coherence tomography," Invest. Ophthalmol. Vis. Sci. **50**(1), 405–413 (2008).

1. Introduction

Assessment of the circulatory system is essential for diagnosing diseases and investigating pathology. Vascular imaging is a powerful tool to assess of the circulatory system. In clinical ophthalmology, however, there are many difficulties in vascular imaging. The eye has one of the most complex vascular systems because of its fine anatomy to form the vision system. Fluorescence angiography is the current standard diagnostic method for assessing circulation in the posterior eye [1], providing detailed visualization of the retinal and choroidal vasculature. However, it has nearly no depth-resolving power due to the property of eye optics and sensitivity [1], making it difficult to access the longitudinal vasculature. There are several other techniques of optical blood flow imaging *in vivo* human posterior eye [2–4]. However, all of them have the same disadvantage of axial resolution. Widely used non-ophthalmic vascular imaging such as computed tomographic and magnetic resonance angiographies [5] and ultrasound sonography are unsuitable because they provide poor resolutions compared to fine structures in the eye.

Angiographic imaging using optical coherence tomography (OCT) [6] is a possible alternative to current methods. OCT with a spectrally resolved detection scheme [7–10] enables high-speed three-dimensional volumetric imaging *in vivo* [11–15]. Volumetric vasculature imaging [16–21] is also enabled by high-speed blood flow detection with OCT [22,23]. High-sensitive angiographic OCTs are recently presented by using Doppler phase shift between successive B-scans or specialized beam-scan pattern [24–27]. However, to obtain high sensitivity, still the options of spatial sampling configuration are limited. This limitation causes the loss of imaging speed and a disadvantage for high-speed and high-sensitive angiography of *in vivo* eye imaging.

In this paper, we developed three-dimensional angiography with high-speed OCT, called optical coherence angiography (OCA) [16], with dual-beam-scan Doppler detection. Time-delayed dual scan with two probes is used to achieve high sensitivity and high speed imaging. We demonstrate the utility of dual-beam-scan Doppler OCA to perform high-speed, high-resolution three-dimensional imaging of the vasculature in the *in vivo* human eye.

#138562 - $15.00 USD Received 24 Nov 2010; revised 7 Jan 2011; accepted 9 Jan 2011; published 14 Jan 2011

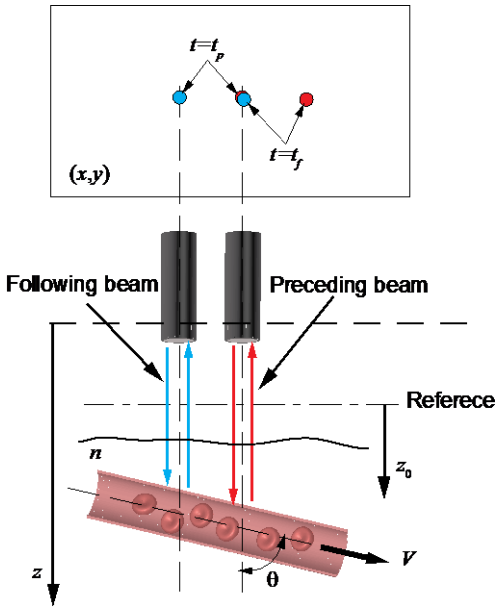

Fig. 1. Dual-beam-scan Doppler flow detection scheme. Two probing beams are focused on the sample at different locations in the (x,y) plane at time $t = t_p$. Probing lights are led into the tissue, which has a refractive index n. The backscattered lights are collected at the emission points. Phases of lights reflected from within a blood vessel that is oriented at angle θ to the propagation direction of the beams are modulated by a Doppler frequency shift since they are scattered by moving scatterers, e.g., red blood cells. By scanning the probes, the following beam at $t = t_f$ reaches the position where the preceding beam was located at $t = t_p$. By comparing the phases of two backscattered lights at the same position with the preceding and following beams, the Doppler frequency shift can be quantified.

2. Method

2.1. Principle of dual-beam-scan Doppler detection

The dual-beam-scan Doppler detection method measures single Doppler frequency shift from two backscattered lights associated with two probing beams. The probes are separated on the sample into the scanning direction and scanned simultaneously (Fig. 1). Through the scanning of probes over the sample surface, electric fields of lights, $E_p(x,y,z,t_p)$, $E_f(x,y,z,t_f)$, are backscattered from a position (x,y,z) of the sample and are collected at different times, t_p, t_f., where the subscripts p and f denotes preceding and following probes respectively. Spectrally-resolved interference signals between collected lights and reference light are detected and Fourier transformed into complex OCT signals [22], $\Gamma_p(x,y,z_0,t_p)$ and $\Gamma_f(x,y,z_0,t_f)$, where $z_0 = z - z_R$ is the path length difference from the reference length z_R. Since motion distribution within the sample causes Doppler frequency shifts $\Delta f(x,y,z_0)$, phases of OCT signals which are obtained from interference signals are modulated over time as $\Gamma_p(x,y,z_0,t_p) = \Gamma_p'(x,y,z_0) \exp[i2\pi\Delta f(x,y,z_0)t_p]$, $\Gamma_f(x,y,z_0,t_f) = \Gamma_f'(x,y,z_0) \exp[i2\pi\Delta f(x,y,z_0)t_f]$, where $\Gamma_p'(x,y,z_0)$ and $\Gamma_f'(x,y,z_0)$ are time independent parts of $\Gamma_p(x,y,z_0,t_p)$ and $\Gamma_f(x,y,z_0,t_f)$. By using the same wavelength band for two probes, we can assume that $\Gamma_p'(x,y,z_0) = \Gamma_f'(x,y,z_0) = \Gamma'(x,y,z_0)$. $\Delta f(x,y,z_0)$ is calculated from the phase difference between $\Gamma_p(x,y,z_0,t_d)$ and $\Gamma_f(x,y,z_0,t_f)$,

$$\Delta f(x,y,z_0) = \frac{1}{2\pi\Delta T} Arg\left[\Gamma_f(x,y,z_0,t_f)\Gamma_p^*(x,y,z_0,t_p)\right], \qquad (1)$$

where $\Delta T = t_f - t_p$ is the time delay. In previous angiographic OCTs, the same point or very close points should be sampled by a single probe at least twice. This requirement heavily limits the options of scanning protocol of angiographic OCTs. Since the dual-beam-scan

#138562 - $15.00 USD Received 24 Nov 2010; revised 7 Jan 2011; accepted 9 Jan 2011; published 14 Jan 2011

Doppler OCA scans exactly same location on the retina twice by using two probe beams, it is free from this limitation of scanning protocol. Furthermore, the detection sensitivity of $\Delta f(x,y,z_0)$ can be increased without decreasing of imaging speed since ΔT, which is in proportion to the Doppler sensitivity from Eq. (1), can be independently adjusted from the scanning protocol by changing the separation of probes and its orientation.

2.2. System configuration

The instrumentation diagram is shown in Fig. 2. Two probing beams are multiplexed in orthogonal polarization states. The light source is a superluminescent diode (SLD-37-HP, Superlum Diodes Ltd., Ireland) with the central wavelength of 840 nm and spectral bandwidth of 50 nm (full width at half-maximum: FWHM). Light source output is propagated in a single-mode (SM) fiber. The light passes through a SM fiber isolator. A polarization controller follows the isolator. The light is split to the fast and slow modes in the polarization-maintaining (PM) fiber (Thorlabs, USA). The interferometer consists of a PM fiber coupler. The splitting ratio of the coupler is 80/20 with 20% going to the sample arm. Two polarization modes are separated by a Wollaston prism in the probing arm. The similar interferometer configuration has presented in the previous study for differential phase contrast imaging [28,29]. The custom-made Wollaston prism (Halbo Optics, UK) has a separation angle of 0.35 degrees. Two polarization modes independently propagate in the system. The separation of two modes on the cornea becomes 0.684 degrees. After passing the eye optics, the two polarization mode form two probe light spots on the retina, and back scattered. The back scatters lights are combined again by the Wollaston prism and introduced to a polarization-sensitive spectrometer through PM fiber. The two backscattered lights from the sample are independently detected by the polarization-sensitive spectrometer which is identical to the previous study [30]. A polarization beam splitter divides the two polarization modes, and two line scan cameras (AViiVA M2 CL 2014, e2V) detect each mode. The acquisition rate of cameras is 27,778 lines/s. A homemade pupil monitor and fixation target are combined with the system to aim at the center of the pupil and stabilize the subject's gaze.

The polarization controller in the SM fiber regulated the polarization state at the connection between the SM and PM fibers to ensure identical optical powers in each mode and the same sensitivity in both polarization channels. The optical power on a sample is 370 μW for each polarization mode. The total power is 740 μW, which is lower than the safe exposure limit according to the ANSI standard (Z136.1). The predicted shot-noise-limited sensitivity is 100 dB with an integration time of 34.8 μs. The sensitivity was measured as 94 and 93 dB for each channel, which was approximately 6 dB lower than the shot-noise-limited sensitivity. This is reasonable since the optical power loss of the system was measured to be 6.5 dB, which may be due to the loss at fiber re-coupling, polarization crosstalk in optical components, the alignment error of the mirror sample for sensitivity measurement because of the difficulty to align the mirror for both separated sampling beams. The beam diameter at $1/e^2$ on the cornea is about 820 μm: the beam spot diameter on the retina is around 13 μm (FWHM). The axial resolution of approximately 8 μm (FWHM) in air is achieved.

#138562 - $15.00 USD Received 24 Nov 2010; revised 7 Jan 2011; accepted 9 Jan 2011; published 14 Jan 2011

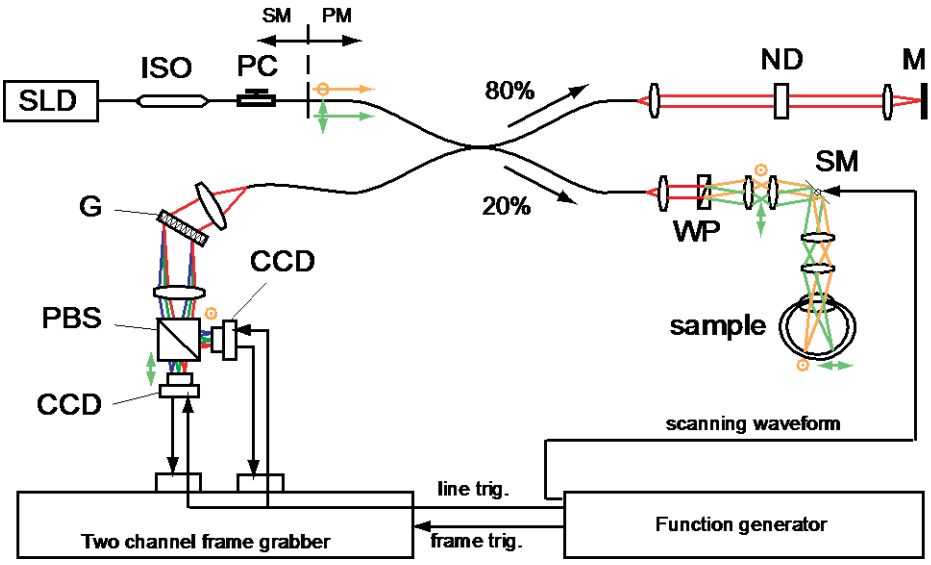

Fig. 2. Dual-beam-scan optical coherence angiography instrumentation. Spectral-domain optical coherence tomography uses a superluminescent diode (SLD). Orthogonal polarization states are separated and independently propagated inside a polarization-maintaining (PM) fiber 80/20 coupler. They are separated spatially on the sample by using a Wollaston prism (WP) and scanned by a scanning mirror module (SM). Reference beams are attenuated by a neutral density filter (ND) and reflected by a mirror (M). The reference arm should exhibit no birefringence to avoid cross-talk between the two channels. Interference signals of each polarization state are detected by a polarization-sensitive spectrometer consisting of a grating (G), polarization beam splitter (PBS), and two line scan CCD cameras (CCD). The cameras are synchronously driven by the same trigger from a function generator through a frame grabber.

A cross coupling between the polarization channels could cause a ghost image in PM fiber-based system [31,32]. However, this ghost image is negligible in our system by the following reasons. (1) In the sample arm, backscattering at the tissue will cause the alteration of the state of polarization, and cross-polarized component generated by the alteration will cause the cross coupling. However, in our system, the Wollaston prism directs the cross-polarized component out of the fiber core, and it does not contribute to the generation of the ghost image. (2) In the reference arm, since there are only a few optical elements and no polarization component, the polarization cross coupling is small. In addition, the extinction ratios of all the polarizing optics are high for the entire bandwidth, because the light source employed in our system is not ultra-broadband. Because of these reasons the cross coupling are reasonably small and the ghost image is negligible.

2.3. Flow image processing

Flow signal is obtained with post-signal processing. Two OCT signals are aligned horizontally and longitudinally. The lateral displacement is corrected by accounting the observation time. Fiber-length-mismatch between the sample and reference arms and its resulting group delay mismatch between two polarization channels of PM fiber causes axial displacement between the two OCT signals. The variance of the phase difference of two OCT signals takes its minimum when this axial displacement was cancelled. In the system calibration process, this displacement was determined by minimizing the phase variance of OCT signals obtained from a static turbid phantom, and numerically cancelled in the true measurement process. Two OCT signals at the same location are obtained. The phase shift between them is provided by using the Kasai auto-correlation $\Delta\varphi(x_i, z_j) = Arg\left[\sum_k^M \sum_l^N \Gamma_f(x_{i+k+n}, z_{j+l}) \Gamma_p^*(x_{i+k}, z_{j+l})\right]$, where Γ_p and Γ_f are axial complex OCT signals obtained by preceding and following probing

#138562 - $15.00 USD Received 24 Nov 2010; revised 7 Jan 2011; accepted 9 Jan 2011; published 14 Jan 2011

beams, respectively, *i* and *j* are indices of pixel, *n* is the number of axial scans in time delay ΔT, and *M* and *N* are lateral and axial window sizes, respectively.

One important post-image processing is removing low signal region. Since the low signal-to-noise ratio exhibits random phase distribution, it disturbs flow images. Doppler phase shift are masked for display by applying a particular threshold to averaged auto-correlation $g\left(x_i, z_j\right) = \frac{1}{MN}\left|\sum_k^M \sum_l^N \Gamma_f\left(x_{i+k+n}, z_{j+l}\right)\Gamma^*_p\left(x_{i+k}, z_{j+l}\right)\right|$. Since this averaging makes g approaching to the population correlation, it will be suppressed and to be zero in the case of completely random noise while maintained for the correlated signals. The threshold level can be set lower and classification accuracy will be high. As for additive white noise, SD-OCT noise is a zero-mean circular Gaussian variable, where the amplitude is a random Rayleigh variable. The probability density distribution of the amplitude of the product of the noise is a double-Rayleigh distribution [33]. The threshold level was determined from the mean $\pi\sigma^2/4$ and deviation $\sqrt{16-\pi^2}\sigma^2/4$ of the amplitude of correlation and the averaging window size *M* and *N* as

$$\Delta\varphi'(x_i, z_j) = \begin{cases} \Delta\varphi(x_i, z_j), & g(x_i, z_j) \geq \left(\frac{\pi}{4} + \alpha\frac{\sqrt{16-\pi^2}}{4}\right)\frac{\sigma^2}{\sqrt{MN}} \\ 0, & otherwise \end{cases} \quad (2)$$

where σ is the standard deviation of amplitude noise in the OCT signal and α is a constant factor set as 4 or 6.

Squared Doppler phase shift is calculated from the result of Eq. (2) and used for qualitative vasculature imaging. Projection images are created by integrating the squared phase shift along the depth. Stereograms, which are pairs of projections from slightly different angle, are provided to show three-dimensional distribution of vasculature. Boundary segmentation algorithm has been applied to separate the retina and the choroid [16].

3. Results

Comprehensive angiography was performed with OCA using dual-beam-scan Doppler detection. The sample was discriminated in three dimensions with the resolution of approximately 15 μm × 30 μm × 6 μm (horizontal sampling separation × vertical sampling separation × and coherence length). Non-invasive three-dimensional microvasculature imaging in the *in vivo* human retina has been demonstrated. The Institutional Review Board of University of Tsukuba approved the experiments. Informed consent was obtained from all volunteers and patients. The probing beams were delivered to the eyes and reached the posterior eye. Backscattered light from the retina and choroid was detected. A healthy eye was scanned over 7.8 × 7.8 mm^2 area with 500 × 256 points around the macula. The total acquisition time was 5 s, marginally suited for *in vivo* human eye imaging. The observation time of motion detection at each point was 396 μs, namely a single point of the retina was scanned twice with this time separation. The volume rendering of three-dimensional flow distribution of a human eye without abnormalities is shown in Fig. 3a. Both the vasculature of the retina and choroid are main supplies to the retina but isolated to each other. Hence it is clinically useful to distinguish them. In Fig. 3a, vessels in the retina and the choroid are distinguished by image segmentation algorithm for OCT images [16] and expressed in different color maps. High-contrast vascular maps in the en-face plane were obtained by projecting three-dimensional squared Doppler flow images (Fig. 3b and 3c). To express the three dimensional structure of two vascular networks, a wall-eyed stereoscopic method was employed (Fig. 3d), where the left pane is for the left eye and the right pane is for the right eye. Different color maps were assigned for the retina and the choroid. Dual-beam-scan Doppler OCA can generate high-contrast retinal and choroidal vascular maps.

#138562 - $15.00 USD Received 24 Nov 2010; revised 7 Jan 2011; accepted 9 Jan 2011; published 14 Jan 2011

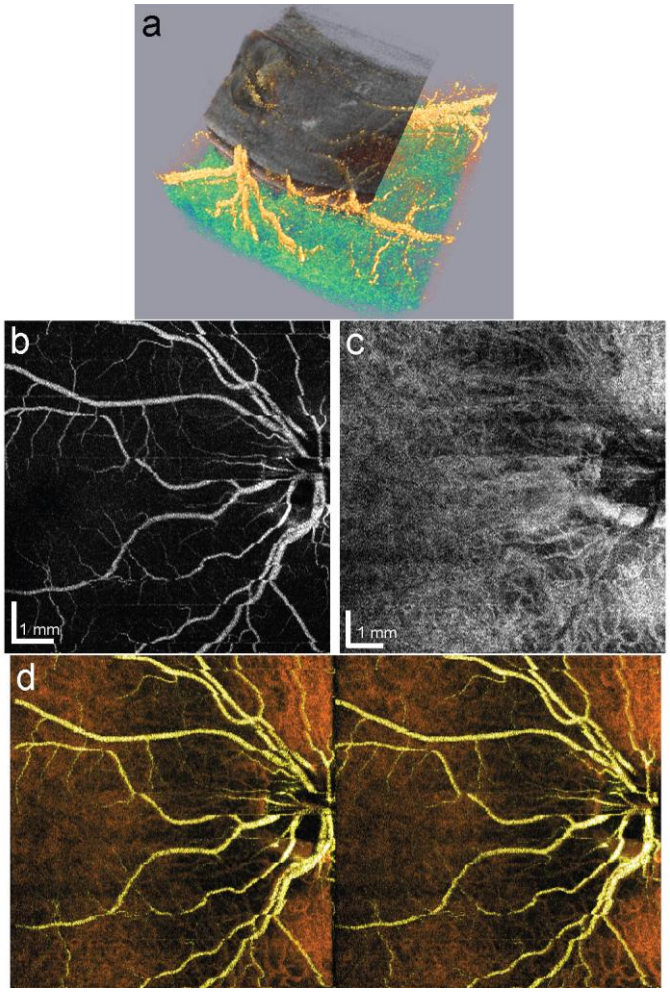

Fig. 3. Dual-beam-scan Doppler optical coherence angiography for the *in vivo* eye. a, A volume-rendering image of the three-dimensional morphology and vasculature of the retina and the choroid. b and c, Projections of flow images at the retina and choroid. d, Wall-eyed stereoview of the retinal (yellow) and choroidal (orange) vasculature. The longitudinal structure and en-face distribution of vessels are shown simultaneously. The scanning area of 30 × 30 degrees (512 × 256 lines) is shown. The observation time of local motion detection ΔT is 396 μs. Acquisition time is around 5 s.

To demonstrate the use of wide-field angiography in the *in vivo* human eye, six sections were scanned to compose wide-field images. The mosaic of vasculature images at the retina and the choroid are shown in Fig. 4a and 4b. Each section was acquired in 5 s and covers an approximate 7.8 × 7.8 mm^2 area. The total acquisition time was 30 s and the mosaic image covers around 16 × 20 mm^2. Owing to the high-resolution three-dimensional imaging, two overlaid vasculatures, the retina and the choroid, can be discriminated. Major retinal vessels around the optic nerve head (ONH) and the macula were observed (Fig. 4a). Fine branches around the fovea were also clearly visualized. In Fig. 4b, the fine choroidal vasculature of the peripapillary region was well contrasted. It shows macroscopic structural properties of vasculature in the posterior eye.

#138562 - $15.00 USD Received 24 Nov 2010; revised 7 Jan 2011; accepted 9 Jan 2011; published 14 Jan 2011

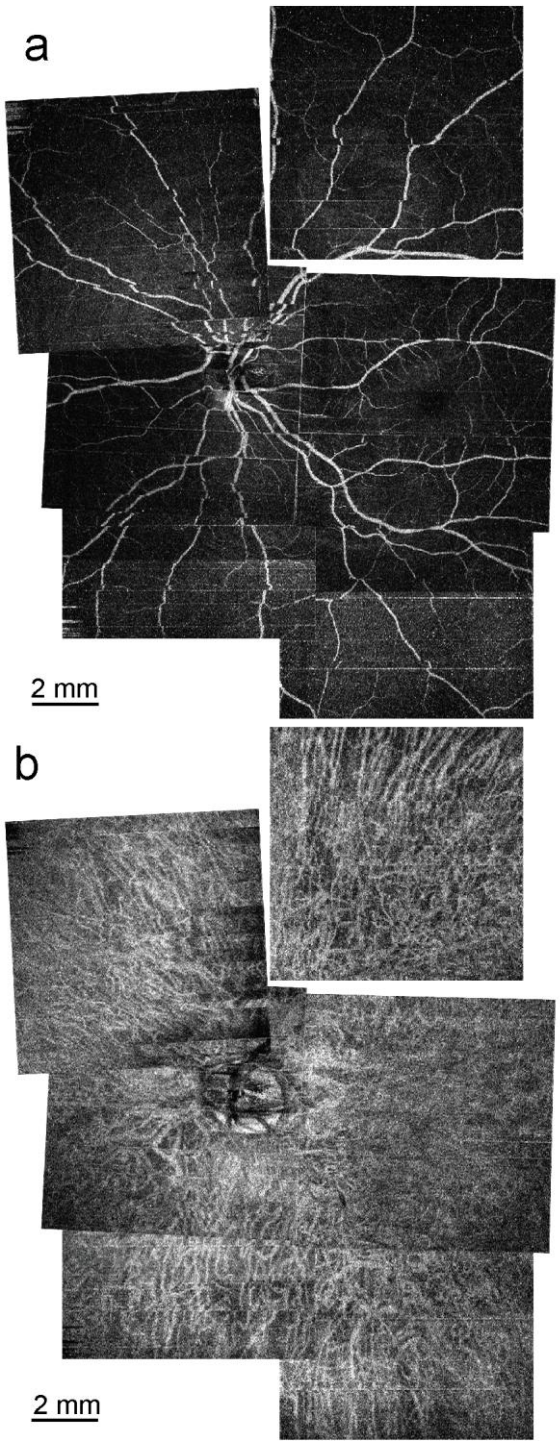

Fig. 4. Wide-field mosaic images of the (a) retinal and (b) choroidal vasculature. Six sessions with scan size of 30 × 30 degrees (512 × 256 lines) comprise the mosaic image. The observation time of local motion ΔT is 396 μs. Acquisition time is around 5 seconds.

#138562 - $15.00 USD Received 24 Nov 2010; revised 7 Jan 2011; accepted 9 Jan 2011; published 14 Jan 2011

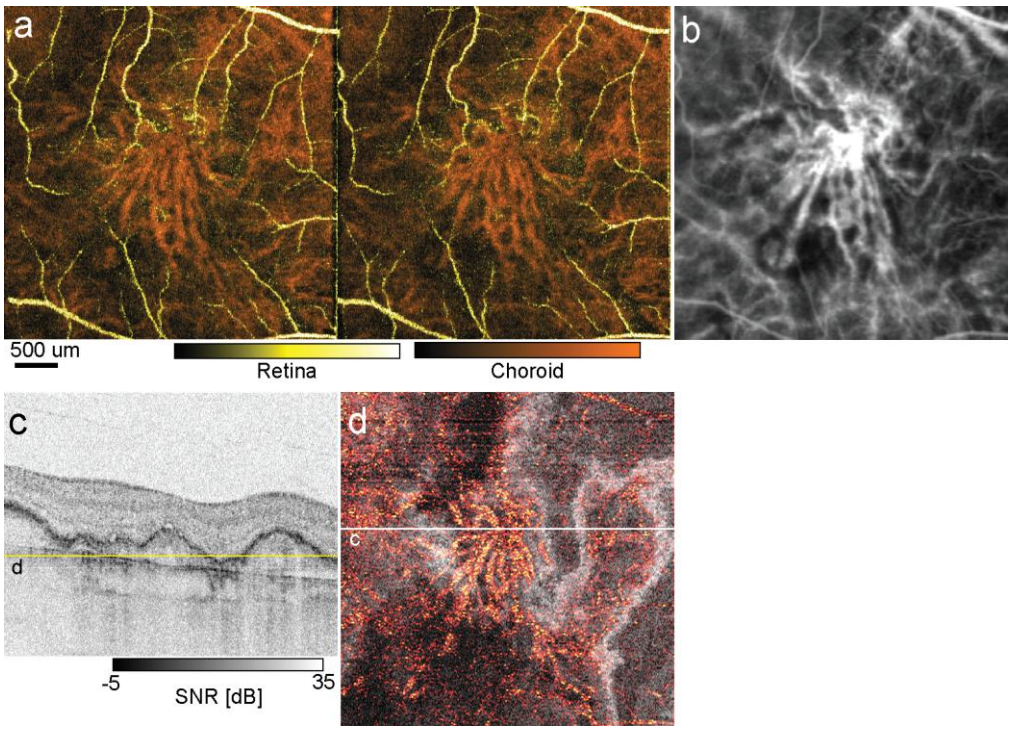

Fig. 5. Abnormal vasculature distribution of a polypoidal choroidal vasculopathy eye. a, Wall-eyed stereoview showing three-dimensional vasculature at a lesion. b, Registered fluorescence image obtained by Indocyanine green angiography (ICGA). c, An OCT image shows the cross-sectional morphology at the lesion (white line in d). d, An en-face cross section of OCT and OCA shows the longitudinal position of the abnormal vasculature (yellow line in c).

Abnormal choroidal vasculature imaging is a significant application for optical coherence angiography [34]. Vasculature imaging has also been used in polypoidal choroidal vasculopathy (PCV) to show the ability of the dual-beam-scan Doppler OCA to the abnormal vasculature investigation. Five pathologic eyes of 4 subjects with PCV were scanned over a 3.9 × 3.9 mm^2 area with 512 × 256 points around the macula. The observation time of Doppler detection was 792 μs, namely, a single location on the retina was scanned twice with the time separation of 792 μs. Abnormal choroidal vascular network and detachment and elevation of the retinal pigment epithelium (RPE) are characteristics of PCV [35,36]. The representative images are shown in Fig. 5. The depth resolved vasculatures can be observed in a stereogram (Fig. 5a). There is a thick abnormal vascular network under the RPE at the fovea. Figure 5a also indicates that the network is located above the surrounding choroidal vessels. Retinal vessels undulated in the longitudinal direction since the retina was elevated. In PCV, polyp-like lesions with pigment epithelium detachment (PED) occur around the abnormal vascular network, visualization of which was provided by the dual-beam-scan Doppler OCA image. In a comparison with Indocyanine green angiography (ICGA) (Fig. 5b), it is found that the remarkable abnormal vasculature generated a similar pattern in both OCA and ICGA images. The longitudinal location of the vascular network can be identified by simultaneously displaying cross-sectional tomography of the eye. A cross-sectional structure of the posterior part is observed by OCT image (Fig. 5c). The RPE was elevated and the complex tissue existed between the RPE and the choroid. In the en-face cross section of the blood flow image overlaid on the OCT image (Fig. 5d), the abnormal vasculature existed at this layer. Although the origin of these abnormal vessels is controversial, dual-beam-scan Doppler OCA will provide a new insight to the debate about this pathology.

#138562 - $15.00 USD Received 24 Nov 2010; revised 7 Jan 2011; accepted 9 Jan 2011; published 14 Jan 2011

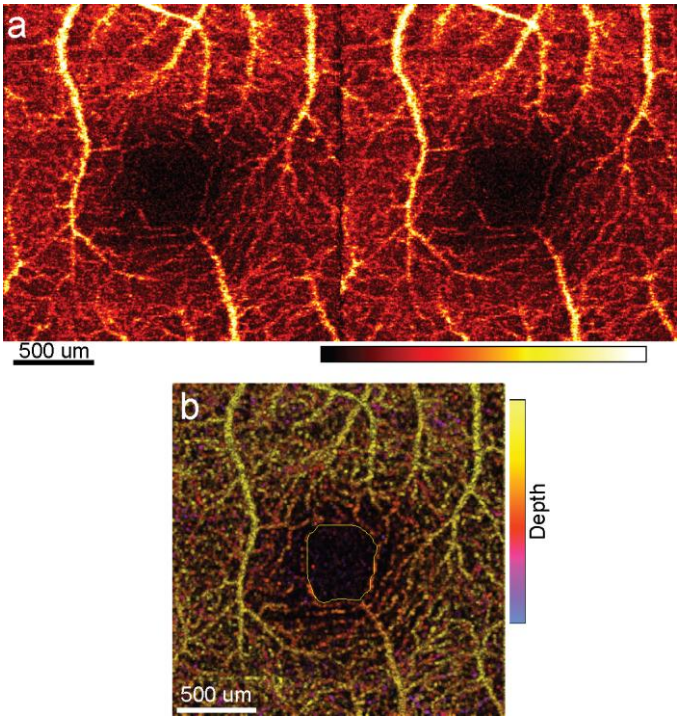

Fig. 6. Three-dimensional retinal capillary imaging. a, Wall-eyed stereoview showing the retinal capillaries obtained by ultrahigh-sensitive blood flow imaging. The scan size is 7.9 × 7.9 degrees (512 × 256 lines). The observation time of local motion ΔT is 1.58 ms. The acquisition time is 5 s. b, The projection image of the retinal capillary with color to encode depth. The foveal avascular zone was outlined manually (yellow closed line).

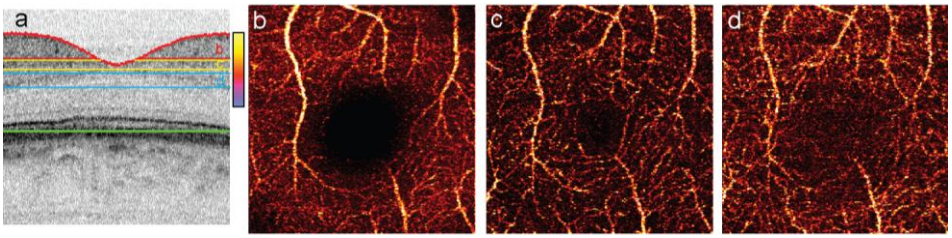

Fig. 7. Retinal capillary networks at different depths. a, An OCT cross section at the fovea. The color map on the right denotes the colors assigned to various depths, as shown in Fig. 6b. Integrated projections of blood flow volume at (b) the ganglion cell layer, (c) the inner plexiform layer to the inner nuclear layer, and (d) the inner nuclear layer to the outer plexiform layer have different capillary networks.

To generate a three-dimensional map of retinal capillaries, the macula around the fovea was scanned. By decreasing the probe scanning speed, the observation time was elongated. This elongated observation time enabled ultrahigh-flow-sensitive imaging. Three eyes of 3 healthy volunteers were scanned over a 1.9 × 1.9 mm^2 area with 512 × 256 points around the macula. The observation time was 1.58 ms. Retinal capillaries around the fovea were visualized in three dimensions by a stereogram (Fig. 6a). The three-dimensional complex and dense capillary network of the macula is shown. In the volume rendering [37] with depth-encoded color map (Fig. 6b), it can be seen that retinal capillaries comprise roughly 3 layers (yellow, orange, and purple vessels). Different patterns of retinal capillary network are confirmed with depth-segmented projections (Fig. 7), a result that is consistent with histological findings [38,39]. The relatively thick retinal vessels are appeared in all segments;

#138562 - $15.00 USD Received 24 Nov 2010; revised 7 Jan 2011; accepted 9 Jan 2011; published 14 Jan 2011

it is perhaps due to the shadowing effect [40]. A region without vasculature is found at the center of the fovea, which is known as the foveal avascular zone (FAZ). Expansion of FAZ is suggested to be an indicator of diabetic retinopathy [41–43]. The FAZ was manually outlined (Fig. 6b, yellow closed line), and the perimeter and area were measured as 1.59 mm and 0.179 mm^2. The results from 3 subjects ranged between 1.59 to 2.42 mm in perimeter and 0.177 to 0.339 mm^2 in surface. They are consistent with a previous study conducted with Fluorescein angiography [43]. Non-invasive, detailed, high-speed imaging of the microvasculature by dual-beam-scan Doppler OCA will be suitable for screening and monitoring of vascular diseases.

4. Discussion

In ophthalmic imaging, fast image acquisition is essential to obtain good image quality. Since live eyes move frequently and quickly, with frequent blinking to condition the cornea, imaging times of less than a few seconds is preferred. Other three-dimensional microvasculature imaging techniques are difficult to perform in living eyes. Doppler ultrasound is slow and has limited resolution due to acoustic attenuation. Photoacoustic microscopy [44] is a promising technique for microvasculature imaging. Its resolution, however, will be limited by acoustic attenuation and laser safety of the eye. Several optical techniques based on confocal microscopy, such as fluorescence confocal microscopy [45], require long acquisition times to collect significant optical power. Previous angiographic OCT using Doppler detection had a trade-off between the sensitivity and the imaging speed. Several previous works improve the sensitivity by using successive B-scans to obtain flow signal or employing specialized scanning pattern [24–27]. The trade-off is mitigated by these method, however still exists for three-dimensional imaging. Not only the observation time for the motion detection but also spatial sampling density is another major factor of flow sensitivity [46,21]. Both limit the speed of high-sensitive, high-resolution vascular imaging. The high sensitivity of flow is preserved by the dual-beam-scan Doppler flow detection with high imaging speed. It provides smooth vascular images in an acquisition time of a few seconds.

FA and ICGA are current clinical standard for ophthalmic angiography. Dual-beam-scan Doppler OCA possesses two evident advantages to these conventional angiographies. First, OCA can assess full three dimensional structure of vasculatures, while FA and ICGA are nominally two-dimensional modalities. Second, OCA is totally non-invasive, while FA and ICGA are known to have moderate but frequent adverse reactions, e.g. nausea, and rare but severe reactions, e.g. anaphylaxes. These two advantages will make OCA as a tool for routine assessment.

Non-invasive comprehensive imaging of posterior eye vasculature by dual-beam-scan Doppler OCA will be suitable for routine monitoring of vascular conditions particularly because of its non-invasiveness. In current clinical ophthalmology, vascular diseases such as age-related macular degeneration are treated with anti-VEGF drugs and/or photodynamic therapy. Although these treatments improve visual acuity, the disease is not cured and symptoms inevitably reoccur. Periodic assessment of the progression of vascular diseases may facilitate better therapeutic management. Further, early detection of abnormal vasculature could enable earlier therapy and protection against the development of some vascular-related diseases. Evaluation of wide-field microvasculature, including longitudinal structures, may reveal tissue activities. Three-dimensional retinal capillary imaging will be a powerful tool not only for retinal disease diagnosis but also for evaluating the whole-body circulatory system. The capillary network changes according to the condition of the vascular system; e.g., hypertension reduces capillary density [47].

In the current system, dual probing beams are provided with mutually orthogonal linear polarization states. Hence, the phase shift between two channels due to birefringence of tissue will be occurred and results in artifacts. The flow images are possibly disturbed at and beneath thick and/or high birefringent tissues, such as thick nerve fiber layer close to the optic nerve head, nerve fiber in the optic disc, and the sclera. The polarization scrambling also causes

#138562 - $15.00 USD Received 24 Nov 2010; revised 7 Jan 2011; accepted 9 Jan 2011; published 14 Jan 2011

phase retardation between two different polarization states [48]. Although the RPE is known to cause polarization scrambling [48], the polarization change at pigments [49] may be caused by scattering, and hence the light passing through the RPE without scattering might not be suffered by the polarization change. Hence the polarization scrambling at the RPE may not affect to choroidal flow imaging. In contrast, choroidal pigments may disturb the flow imaging.

Fast bulk eye motion such as saccade can cause large shift between two channels laterally and longitudinally. The shift due to the bulk motion decreases correlation between two channels and results in increased phase shift noise. During *in vivo* eye imaging, flow images were corrupted if saccade occurred. However, if the shift is only along axial and beam separation directions, it could be compensated by post-image registration.

At the macula, very rich choroidal perfusion and dense network of fine vessels are expected. Perhaps due to resolution limitations, the capillary network in the choroid was not resolved in current dual-beam-scan Doppler OCA images. To visualize large choroidal vessels, more high penetration to the choroid will be needed. The combination of recently developed high-penetration OCT with 1-um wavelength probe [50,51] and the dual-beam-scan scheme may enable the visualization of large choroidal vessels in the future.

5. Conclusion

We demonstrated a method for non-invasive high-speed three-dimensional imaging of microvasculature by using dual-beam-scan Doppler OCA. *In vivo* three-dimensional microvasculature of the posterior part of the human eye had been acquired within a few seconds. Dual-beam-scan Doppler OCA will be a powerful complementary tool of ophthalmic diagnosis for vascular diseases. Furthermore, this high-speed non-invasive angiography might be a potential screening method for vascular-related diseases.

Conventional techniques remain limited for vasculature imaging. On the other hand, the investigation of the dynamics of blood flow is fundamental for a comprehensive assessment of the circulatory system, and it requires high-speed, high-sensitivity, and high-resolution flow measurement. The dual-beam-scan method is able to provide these three requirements simultaneously. Further improvements of the acquisition system, particularly in its speed, will enable four dimensional imaging of microvessel perfusion and further assessment of circulatory system.

Acknowledgements

This research is partially supported by Japan Science and Technology Agency through the contract of Development of Systems and Technology for Advanced Measurement and Analysis.

#138562 - $15.00 USD Received 24 Nov 2010; revised 7 Jan 2011; accepted 9 Jan 2011; published 14 Jan 2011